

RSC Advances



This is an *Accepted Manuscript*, which has been through the Royal Society of Chemistry peer review process and has been accepted for publication.

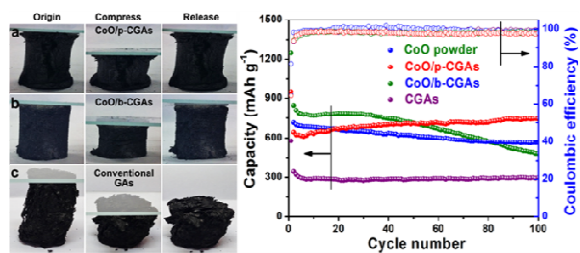
Accepted Manuscripts are published online shortly after acceptance, before technical editing, formatting and proof reading. Using this free service, authors can make their results available to the community, in citable form, before we publish the edited article. This *Accepted Manuscript* will be replaced by the edited, formatted and paginated article as soon as this is available.

You can find more information about *Accepted Manuscripts* in the [Information for Authors](#).

Please note that technical editing may introduce minor changes to the text and/or graphics, which may alter content. The journal's standard [Terms & Conditions](#) and the [Ethical guidelines](#) still apply. In no event shall the Royal Society of Chemistry be held responsible for any errors or omissions in this *Accepted Manuscript* or any consequences arising from the use of any information it contains.

Graphic Abstract

Binder-free electrodes have been synthesized by coupling compressible graphene aerogels with CoO nanostructures, which exhibit superior electrochemical performance to conventional electrodes made of powders and binders in lithium-ion batteries.



COMMUNICATION

Compressible graphene aerogel supported CoO nanostructures as binder-free electrode for high-performance lithium-ion batteries

Cite this: DOI: 10.1039/x0xx00000x

Received 00th January 2012,
Accepted 00th January 2012

DOI: 10.1039/x0xx00000x

www.rsc.org/

Yanfeng Dong, Shaohong Liu, Zhiyu Wang,* Yang Liu, Zongbin Zhao,* and Jieshan Qiu*

Compressible graphene aerogels (CGAs) supported CoO nanostructures were synthesized via hydrothermal strategy. Benefited from good mechanical stability, they can be directly used as binder-free electrodes in lithium-ion batteries, which exhibit superior electrochemical performance to conventional electrodes made of powders and binders.

Lithium-ion batteries (LIBs) have become the predominant power source for portable electronics for many years in virtue of high energy density, long lifespan and environmental benignity.¹⁻⁴ The continuously surging demand in large-scale energy applications such as electric vehicles further boosts great interests in developing high-performance electrode materials that can store more energy efficiently. Among the available alternatives, cobalt oxides (mainly CoO and Co₃O₄) have been regarded as very appealing substitute of conventional graphite anodes because of the high capacity (716 mA h g⁻¹ for CoO and 892 mA h g⁻¹ for Co₃O₄) for lithium storage.^{5,6} However, the reversible conversion reaction between lithium ions and cobalt oxides adversely causes fast capacity fading due to drastic volume change and severe destruction of the electrode during cycling. The sluggish reaction kinetics and poor conductivity of cobalt oxides also induces additional performance degradation of the electrodes, especially at high current rate.⁵

So far, enormous efforts have been devoted to improve the electrochemical properties of cobalt oxides by engineering the nanostructures with optimized particle size, shape and composition.^{5,7-13} However, suffering from low thermodynamic stability, particulate nanostructures tend to self-aggregate during deep cycling, resulting in severe electric isolation between electrode components that inevitably reduces the electrode conductivity. Auxiliary additives such as polymer binders (e.g., polyvinylidene fluoride, PVDF) and conductive agents (e.g., carbon black) have been used to enhance mechanical stability and electronic conductivity of the electrodes. But they adversely reduce battery performance with undesirable inactive volume and side reaction during lithium storage.¹⁴ Recently, the integrated electrodes, where the nanostructures of active materials are conformably coated on or

embedded into free-standing carbon matrix, have been demonstrated with ultrafast power rate and long lifespan.^{15, 16} Successful integration of sturdy carbon support with well-designed nanostructures not only improves the electrode performance, but provides the battery with robust mechanical flexibility and enhanced energy density, rendering this type of electrodes very attractive for deformation-tolerant power sources.

Graphene has been counted as very appealing carbon matrix to support guest materials because of the good conductivity, large surface area, high stability and unique 2D sheet-like structure. However, individual graphene sheets usually tend to restack as a result of strong π - π interactions and van der Waals force between them, which reduces its operational properties and processability. To overcome this problem, various graphene aerogels (GAs) with rich porosity and large surface area have been employed to support active materials for energy storage.¹⁷⁻²⁰ Unfortunately, the pristine GAs tends to collapse or distortion under compression due to the fragile structure, which hindered their application in binder-free electrode in LIBs.²⁰⁻²³

Herein, we report the construction of high-performance binder-free electrode by coupling CoO nanostructures with robust highly compressible GAs (denoted as CGAs). By tuning the surface characteristics of graphene, various CoO nanostructures including the nanowires and urchin-like spheres can be grown on CGAs to form free-standing, easy handling macroassemblies. The excellent mechanical stability and flexibility of CGAs, even after CoO loading, enables them to withstand the electrode preparation and huge volume expansion of the electrode during lithium insertion. Therefore, CoO/CGAs macroassemblies can be directly used as binder-free electrodes in LIBs, exhibiting stable capacity retention for 100 cycles with high capacities and excellent high-rate capabilities. Such free-standing electrodes avoid the use of auxiliary additives in the electrode and heavy metal current collectors (e.g., Cu and Al foils), thus enhancing the overall energy density of the batteries. Their high compressibility may be further beneficial to the volumetric energy density of the batteries.

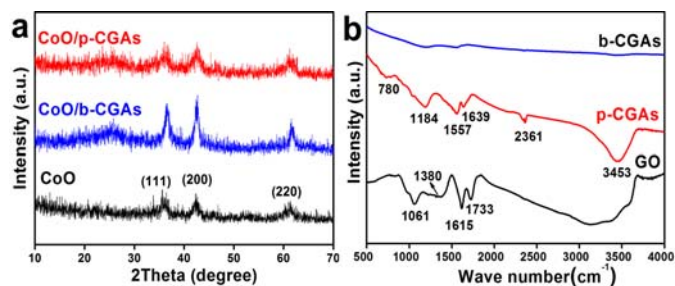


Fig. 1 (a) XRD patterns of CoO/p-CGAs, CoO/b-CGAs macroassemblies and the powder of CoO nanostructure; (b) FTIR spectra of GO, p-CGAs and b-CGAs macroassemblies.

The synthesis of CoO/CGAs electrodes involves two steps. Polypyrrole functionalized CGAs (denoted as p-CGAs) are firstly fabricated via hydrothermal self-assembly of graphene oxide (GO) in the presence of pyrrole, followed by freeze drying. The conjugated structure of pyrrole allows it easily attach to GO surface by hydrogen bonding or π - π interaction. This feature not only prevents the self-stacking of resultant reduced graphene oxide (rGO) sheets, but interlocks individual rGO sheets together to form macroassemblies with high mechanical strength and compressibility. Even after the removal of chemical groups by annealing in N_2 flow, the robust structure of CGAs can still be well maintained, leading to the formation of CGAs with bare surface (denoted as b-CGAs). The robust structure of both CGAs provides the feasibility for loading CoO nanostructures by hydrolysis of cobalt salts and subsequent thermal conversion. It eventually results in CoO/p-CGAs and CoO/b-CGAs macroassemblies as binder-free electrodes in LIBs.

The crystallographic structure and phase purity of CoO/p-CGAs is determined by X-ray powder diffraction (XRD), as shown in Fig. 1a. The broad peak appears at 26° can be ascribed to (002) reflection of stacked graphene sheets.^{18, 25} The formation of CoO is revealed by three pronounced peaks at 36.5° , 42.5° and 61.5° , which can be assigned to the reflection from (111), (200) and (220) planes of cubic CoO (JCPDS 42-1300). No peaks from the impurities such as $Co(OH)_2$ or Co_3O_4 are identified. TGA analyses reveal that the loading amount of CoO in CoO/p-CGAs and CoO/b-CGAs is ca. 51.6 wt. % and 52.7 wt. %, respectively (Fig. S1).

The surface properties of GO, p-CGAs and b-CGAs are examined by Fourier transform infrared spectrometer (FTIR), as shown in Fig. 1b. In the spectrum of GO, the absorption peaks at 1723 cm^{-1} , 1380 cm^{-1} , 1061 cm^{-1} and 1615 cm^{-1} can be ascribed to stretching vibrations of C=O, -OH, carbonyl C-O bonds and C-C aromatic ring modes, respectively.²⁶ The broad absorption peaks at $3000\text{--}3600\text{ cm}^{-1}$ correspond to the O-H stretching vibrations of hydroxyl groups on GO surface and adsorbed water molecules. After the reaction with pyrrole, the intensity of these peaks from oxygen-containing groups is greatly suppressed, while new peaks arise at 1557 cm^{-1} , 1184 cm^{-1} , 780 cm^{-1} and 963 cm^{-1} that can be assigned to typical polypyrrole ring vibrations and C-N stretching vibration for the formation of polymerized pyrrole.^{27, 28} The presence of N atoms has known to facilitate the chemical binding of metal atoms via coordination to them with lone-pair electrons, thus providing sufficient active site for the growth of CoO nanostructures.^{29, 30} After annealing at 800°C , however, almost all the peaks from chemical groups disappeared, leaving bare carbon surface with poor material compatibility to foreign materials. Raman spectra of GO, p-CGAs and b-CGAs is shown in Fig. S2, in which the

intensity ratios between D-band and G-band (I_D/I_G) is used to identify the structural variation of GO. The I_D/I_G value changes from 0.90 to 0.99 for b-CGAs due to partially reduction of GO. For p-CGAs, the I_D/I_G value significantly increases to 1.07, indicating that oxygen-containing groups in GO is effectively removed and subsequently more defects are formed, which is consistent with FTIR result.

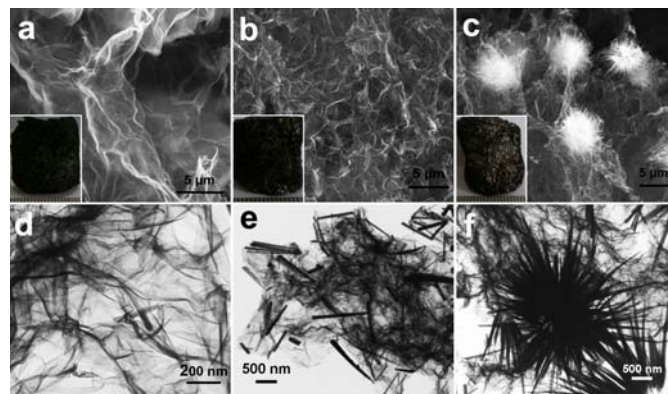


Fig. 2 SEM images of (a) p-CGAs, (b) CoO/p-CGAs and (c) CoO/b-CGAs macroassemblies; their corresponding TEM images are shown in Fig. 2d, Fig. 2e and Fig. 2f, respectively.

A panoramic view by scanning electron microscopy (SEM) reveals that p-CGAs have a foam-like structure with interconnected pores ranging from hundreds of nanometers to few micrometres (Fig. 2a). The graphene walls in p-CGAs are almost transparent under electron irradiation of TEM (Fig. 2d). The robust structure of p-CGAs allows their porosity to be retained after the growth of CoO nanowires with an average diameter of 100 nm and length up to 5 μm (Fig. 2b and Fig. 2e). The ends of these nanowires well contact with rGO surface, indicating the intimate interactions between them. However, when b-CGAs are employed, urchin-like spheres with a size of 4-5 μm are obtained on graphene walls by self-assembly of CoO nanowires under the same conditions (Fig. 2c and Fig. S2). The distinct shape of CoO nanostructures can be explained by the growth behaviour of CoO crystals on graphene with different surface characteristics. On p-CGAs, the presence of chemical groups provides sufficient active site for the absorption of cobalt ions, as well as heterogeneous nucleation and anisotropic growth of CoO nanowires. While for b-CGAs, homogenous nucleation of CoO in solution is preferred due to the weak interaction between CoO crystals and bare graphene. In this case, urchin-like assembly of CoO nanowires is formed to reduce the total surface free energy of the nanostructures.

Regardless the structure of CoO, both CoO/p-CGAs and CoO/b-CGAs macroassemblies exhibit excellent mechanical compressibility, as shown in Fig. 3. They can be easily squeezed into a pellet under pressure but recover from strain as high as 50%. Once the external pressure is removed, they unfold almost completely, while the conventional GAs recovers only partially and severe collapse happens simultaneously. The high compressibility of CGAs is the result of the compact junctions among rGO sheets in CGAs.^{18, 31, 32} This unique feature makes it possible to produce free-standing electrodes for lithium storage by simply cutting the CoO/CGAs macroassemblies to round pieces. Fig. 4a shows the typical discharge/charge profiles of CoO/p-CGAs electrodes at the 1st, 20th, 50th and 100th cycles. They deliver an initial discharge and charge specific capacity of 951 and 612 mA h g^{-1} . The

irreversible capacity loss of 35 % is due to the irreversible process such as the formation of SEI films and trap of the lithium in crystal lattice. From second cycle onwards, CoO/p-CGAs electrodes exhibit stable capacity retention of 100 % with a high capacity of 743 mA h g^{-1} at a current density of 100 mA g^{-1} . This value is slightly higher than the theoretical value for CoO/graphene composite ($C = C_{\text{CoO}} \times W_{\text{CoO}} + C_{\text{graphene}} \times W_{\text{graphene}} = 727.2 \text{ mA h g}^{-1}$; C and W is defined as the theoretical capacity and weight ratio of labelled materials), showing high utilization of the active materials. The capacity rise throughout the cycling is not uncommon for cobalt oxides because of the reversible formation of organic polymeric/gel-like layer by the decomposition of the electrolyte and the activation of the active materials.^{2, 33, 34} For CoO/b-CGAs electrodes, they exhibit an initial discharge and charge specific capacity of 925 and 755 mA h g^{-1} with an irreversible capacity loss of 18.4 %. After 100 cycles, a lower but comparable charge capacity of 544 mA h g^{-1} can be achieved, corresponding to a capacity retention of 72 %. With the aim of demonstrating the advantages of CoO/CGAs electrodes on lithium storage, the cycling performance of the electrode made from the powders of CoO nanostructures, as well as the CGAs electrodes, are also investigated under the same conditions. The former shows fast capacity decay in 40 cycles while GAs electrodes deliver very low capacity of 300 mA h g^{-1} throughout 100 cycles. Apparently, the unique combination of CoO nanostructure and CGAs can significantly improve the electrochemical properties of CoO-based electrodes.

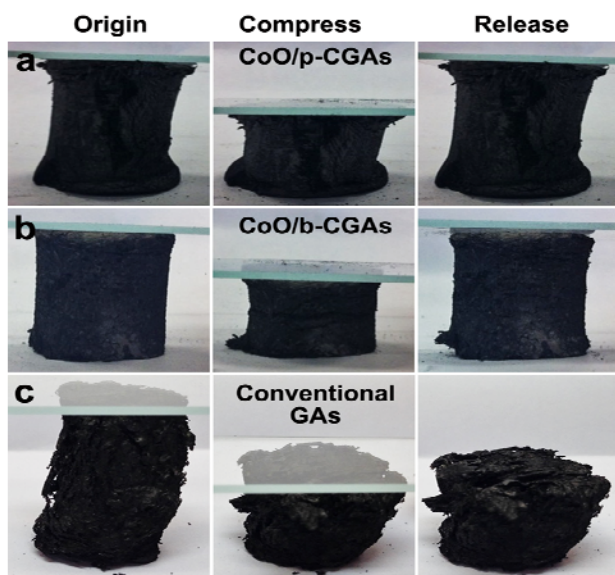


Fig. 3 Optical images showing high compressibility of (a) CoO/p-CGAs, (b) CoO/b-CGAs macroassemblies and (c) the fragility of conventional GAs.

Benefitted from unique structure, CoO/p-CGAs electrodes also exhibit excellent cycling response to continuously varying current rates although cobalt oxides are generally observed to suffer from sluggish kinetics. Even cycled at high current densities of 300 to 3000 mA g^{-1} , comparable capacities of 125 - 649 mA h g^{-1} can still be reserved, as shown in Fig. 4d. After deep cycling at 3000 mA g^{-1} , stable high capacity could be largely restored for repeated cycles after abruptly switching the current density back to 300 mA g^{-1} , indicating the excellent robustness and stability of the electrode. As a comparison,

CoO/b-CGAs electrodes and CoO powder electrodes exhibit fast capacity fading with current density increasing and most of the capacities are lost at high current densities of 1000 - 2000 mA g^{-1} . When cycled back to 300 mA g^{-1} , apparent capacity fading is observed due to poor electrode stability during repeatedly discharge/charge cycles.

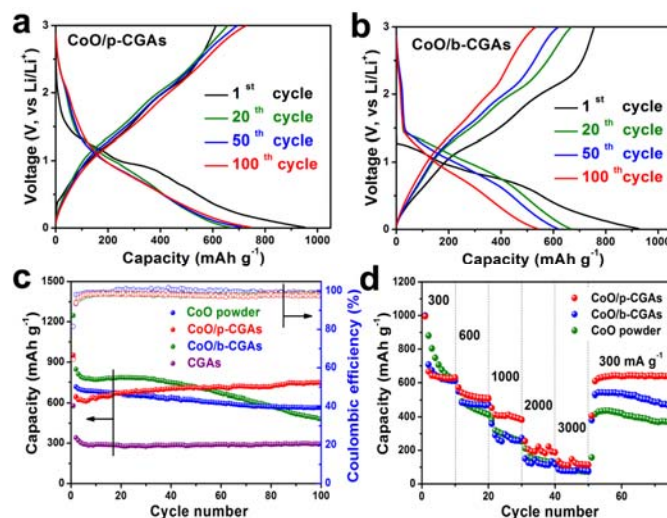


Fig. 4 Discharge/charge profiles of (a) CoO/p-CGAs and (b) CoO/b-CGAs electrodes at the current of 100 mA g^{-1} ; (c) cycling performance of CoO/p-CGAs, CoO/b-CGAs, CoO powder and CGAs electrodes; (d) rate capability of CoO/p-CGAs, CoO/b-CGAs and CoO powder electrodes at various current densities.

The excellent electrochemical performances of CoO/p-CGAs electrodes closely rely on their unique structures. First, nanowire structure greatly shortens the ionic diffusion length and provides sufficient electrode-electrolyte contact area for lithium storage reactions in CoO.^{35, 36} They are grown firmly on graphene sheets without aggregation, thus can be fully accessible by Li^+ in the electrolyte. In conventional electrodes made from powders, however, severe agglomeration of the nanostructures is likely to occur and largely eliminate the active interface. Moreover, the CGAs also play an important role to enhance the electrode conductivity by forming a continuous 3D electronic path for fast and stable charge transfer, as characterized by electrochemical impedance spectroscopy (EIS) (Fig. S3), while granting the electrode with large surface area, high porosity, high mechanical flexibility and stability. Their high compressibility also helps to enhance the volumetric energy density of the cells when being compressed. The integration of all these advantageous features makes CoO/CGAs electrodes highly attractive for deformation-tolerant power sources and electronic devices.

Conclusions

In summary, CoO/CGAs macroassemblies have been successfully synthesized by hydrothermal growth of various CoO nanostructures on compressible graphene aerogels with tuneable surface characteristics. The morphology of CoO nanostructures on CGAs can be tailored by tuning the surface chemistry of CGAs, yielding uniform CoO nanowires or urchin-like CoO spheres. Benefitted from unique structural merits, CoO/CGAs macroassemblies could serve as binder-free anodes for LIBs to exhibit excellent cycle stability for over 100 cycles and good rate capability at high current rate of up to

3000 mA g⁻¹. The present strategy may shed some light on the construction of binder-free, easy-handling electrodes for deformation-tolerant LIBs.

Acknowledgements

This work was partly supported by the National Natural Science Foundation of China (No. 51072028). Z. W. acknowledges the support from the Recruitment Program of Global Youth Experts (2014) and the start-up grant from Dalian University of Technology (No. 1000-852036).

Notes and references

Carbon Research Laboratory, Liaoning Key Lab for Energy Materials and Chemical Engineering, State Key Lab of Fine Chemicals, School of Chemical Engineering, Dalian University of Technology, Dalian 116023, China.

Email: zywang@dlut.edu.cn; zbzha@dlut.edu.cn; jqiu@dlut.edu.cn

Electronic Supplementary Information (ESI) available: the experimental details, more TGA, SEM and electrochemical data. See DOI: 10.1039/c000000x/

- A. S. Arico, P. Bruce, B. Scrosati, J.-M. Tarascon and W. van Schalkwijk, *Nat Mater*, 2005, **4**, 366.
- Z. Wang, D. Luan, S. Madhavi, Y. Hu and X. W. Lou, *Energy & Environmental Science*, 2012, **5**, 5252.
- L. Ji, Z. Lin, M. Alcoutlabi and X. Zhang, *Energy & Environmental Science*, 2011, **4**, 2682.
- L. Zhang, G. Zhang, H. B. Wu, L. Yu and X. W. Lou, *Advanced Materials*, 2013, **25**, 2589.
- H. Guan, X. Wang, H. Li, C. Zhi, T. Zhai, Y. Bando and D. Golberg, *Chemical Communications*, 2012, **48**, 4878.
- S. Xiong, J. S. Chen, X. W. Lou and H. C. Zeng, *Advanced Functional Materials*, 2012, **22**, 861.
- X. Guan, J. Nai, Y. Zhang, P. Wang, J. Yang, L. Zheng, J. Zhang and L. Guo, *Chemistry of Materials*, 2014, **26**, 5958.
- Y. Sun, X. Hu, W. Luo and Y. Huang, *Journal of Materials Chemistry*, 2012, **22**, 13826.
- M. Zhang, F. Yan, X. Tang, Q. Li, T. Wang and G. Cao, *Journal of Materials Chemistry A*, 2014, **2**, 5890.
- W. Yuan, J. Zhang, D. Xie, Z. Dong, Q. Su and G. Du, *Electrochimica Acta*, 2013, **108**, 506.
- K. Xie, P. Wu, Y. Zhou, Y. Ye, H. Wang, Y. Tang, Y. Zhou and T. Lu, *ACS applied materials & interfaces*, 2014, **6**, 10602.
- C. Peng, B. Chen, Y. Qin, S. Yang, C. Li, Y. Zuo, S. Liu and J. Yang, *ACS nano*, 2012, **6**, 1074.
- Z. Wang, Z. Wang, W. Liu, W. Xiao and X. W. Lou, *Energy & Environmental Science*, 2013, **6**, 87.
- G. Zhou, F. Li and H.-M. Cheng, *Energy & Environmental Science*, 2014, **7**, 1307.
- S. Liu, Z. Wang, C. Yu, H. B. Wu, G. Wang, Q. Dong, J. Qiu, A. Eychmüller and X. W. Lou, *Advanced Materials*, 2013, **25**, 3462.
- N. Li, Z. Chen, W. Ren, F. Li and H.-M. Cheng, *Proceedings of the National Academy of Sciences*, 2012, **109**, 17360.
- H. Hu, Z. Zhao, W. Wan, Y. Gogotsi and J. Qiu, *Advanced Materials*, 2013, **25**, 2219.
- Y. Zhao, C. Hu, Y. Hu, H. Cheng, G. Shi and L. Qu, *Angewandte Chemie*, 2012, **124**, 11533.
- Y. Gong, S. Yang, Z. Liu, L. Ma, R. Vajtai and P. M. Ajayan, *Advanced Materials*, 2013, **25**, 3979.
- W. Chen, S. Li, C. Chen and L. Yan, *Advanced Materials*, 2011, **23**, 5679.
- L. Xiao, D. Wu, S. Han, Y. Huang, S. Li, M. He, F. Zhang and X. Feng, *ACS applied materials & interfaces*, 2013, **5**, 3764.
- W. Wei, S. Yang, H. Zhou, I. Lieberwirth, X. Feng and K. Müllen, *Advanced Materials*, 2013, **25**, 2909.
- Y. Huang, D. Wu, S. Han, S. Li, L. Xiao, F. Zhang and X. Feng, *ChemSusChem*, 2013, **6**, 1510.
- H. Hu, Z. Zhao, Q. Zhou, Y. Gogotsi and J. Qiu, *Carbon*, 2012, **50**, 3267.
- H. Chen, M. B. Müller, K. J. Gilmore, G. G. Wallace and D. Li, *Advanced Materials*, 2008, **20**, 3557.
- S. Park, K.-S. Lee, G. Bozoklu, W. Cai, S. T. Nguyen and R. S. Ruoff, *ACS nano*, 2008, **2**, 572.
- C. Xu, J. Sun and L. Gao, *Journal of Materials Chemistry*, 2011, **21**, 11253.
- L. L. Zhang, S. Zhao, X. N. Tian and X. S. Zhao, *Langmuir*, 2010, **26**, 17624.
- Y. Liang, Y. Li, H. Wang, J. Zhou, J. Wang, T. Regier and H. Dai, *Nature Materials*, 2011, **10**, 780.
- Y. Liang, H. Wang, J. Zhou, Y. Li, J. Wang, T. Regier and H. Dai, *Journal of the American Chemical Society*, 2012, **134**, 3517.
- Y. Zhao, J. Liu, Y. Hu, H. Cheng, C. Hu, C. Jiang, L. Jiang, A. Cao and L. Qu, *Advanced Materials*, 2013, **25**, 591.
- Y. Xu, K. Sheng, C. Li and G. Shi, *ACS nano*, 2010, **4**, 4324-4330.
- P. Poizot, S. Laruelle, S. Grugeon, L. Dupont and J. M. Tarascon, *Nature*, 2000, **407**, 496.
- S. Laruelle, S. Grugeon, P. Poizot, M. Dollé, L. Dupont and J.-M. Tarascon, *Journal of The Electrochemical Society*, 2002, **149**, A627.
- X. Xia, J. Tu, Y. Zhang, X. Wang, C. Gu, X.-b. Zhao and H. J. Fan, *ACS nano*, 2012, **6**, 5531.
- Y. Li, B. Tan and Y. Wu, *Nano letters*, 2007, **8**, 265.